Chapter 5

The Nucleus of Comet Encke

5.1 Background

Comet 2P/Encke has been observed by mankind since 1786. Of the roughly 150 known periodic comets that have not been lost, only four others have an observational baseline as long. The comet was discovered independently four times, once each on four different apparitions, before J. F. Encke published an orbit connecting them all and successfully predicting the next apparition. The orbital period is 3.3 years, the shortest known, and so at first glance one would think that it would be the comet we know the most about. In some aspects this is true – e.g. Whipple and Sekanina (1979) and Sekanina (1988a,b) have a detailed model of the nucleus' rotation – but the comet furtively guarded the basic properties of its nucleus until the 1997 apparition, when it made its closest recorded passage to Earth ever. We set up a multiwavelength observing campaign to take advantage of this opportunity. I have described much of this experiment elsewhere (Fernández *et al.* 1999c) and reproduce much of the text.

5.2 Observations and Reduction

The three datasets used in this study are described in Table 5.1, along with heliocentric distances, geocentric distances, and phase angles. The measured fluxes are given in Table 5.2. Images from the European Southern Observatory (ESO) 3.6-m telescope were taken with the TIMMI instrument (Käufl *et al.* 1994) at wavelengths between 8 and 12 μm. The images have 64^2 pixels and cover $(21.8'')^2$. Each pixel width covered 65 to 87 km at the comet during the observing run. The plate scale was measured using the known relative positions of α Cen A and B (Perryman *et al.* 1997). The point-spread function's (PSF) full width at half-maximum (FWHM) varied from 0.7 to 1.0 arcsec. Chopping of the secondary mirror northward and nodding of the telescope westward, with typical throws of 30 arcsec, were employed. An array flat field was created by measuring the relative photometry of a bright star at 23 different locations on the array and then interpolating a surface with a minimum of curvature. We observed the comet at three wavelengths but only at $\lambda = 10.7$ μm was the comet bright enough to let us build a well-sampled time series of data. Absolute flux calibration was done using α Cen A and interpolating in wavelength information given by van der Bliek *et al.* (1996); its 10.7 μm magnitude is -1.56 ± 0.05, and the zero point is at 35.7 Jy. Color corrections were at most a few percent. Relative flux calibration was done using SAO 243305 = HD 143796 = V362 Nor (Kazarovets *et al.* 1999), a star that was a short angular distance from the comet and thus useful for measuring the atmospheric effects and the comet's light curve. Its optical variability is $\leq \pm 0.05$ mag with sporadic ~ 0.1 mag jumps every few years (Perryman 1997). There was no indication of variability in the mid-IR data that exceeded photometric uncertainty.

The *Infrared Space Observatory* (*ISO*) data, taken with the ISOPHOT instrument (Lemke *et al.* 1996), used a 180-arcsec wide circular aperture at wavelengths between 3.6 and 100 μm. The data were reduced using the "PIA" software version 7.1 (Gabriel *et al.* 1997). Corrections to the measured fluxes were made to account for the nonlinearities in the detector, the diffraction of light beyond the aperture, and the color of the flux standard vis-à-vis the comet; these corrections were at most 3%.

The *Hubble Space Telescope* (*HST*) images were taken with the CCD on the Space Telescope Imaging Spectrograph (STIS; Woodgate *et al.* 1998) as acquisition images for a separate spectroscopic program. A ~5500 Å-wide red filter was used. We used the science-quality output of the pipeline processing of the data. Each pixel covers $(0.051'')^2$, or $(7.4 \text{ km})^2$ at the comet. The high proper motion of the comet ($\sim 0.2''$ per second) left all stars as trails; we estimate that the PSF FWHM= $0.1''$ based on archival *HST* images taken with the same instrument, detector, and filter within a few weeks of our observations.

5.3 Analysis

5.3.1 ESO Photometry

Figure 5.1a shows the median of 61 ESO TIMMI images of the comet, with a linear intensity scale. Each image was weighted by the total signal. The total

Table 5.1. Observations of Comet Encke

No.	Date (UT)	System	Wavelength (μm)
1	1.3 Jul 1997	*HST* + STIS	0.72
2	15.0 Jul 1997	*ISO* + ISOPHOT	3.6 - 100
3	15.0-21.1 Jul 1997	ESO 3.6-m + TIMMI	8.5 - 11.6

No.	r (AU)	Δ (AU)	α ($^\circ$)
1	0.942	0.200	106.2
2	1.164	0.264	50.3
3	1.164-1.257	0.264 - 0.351	50.3 - 40.3

Table 5.2. Flux of Comet Encke

Wavelength (μm)	Filter Name	Filter Width[a] (μm)	Aperture Radius ($''$)	Flux (Jy)
ESO[b]				
8.5	"N1"	0.9	3	2.5 ± 0.7
10.7	"NN1"	1.2	3	3.1 ± 0.2
11.6	"SiC"	1.6	3	2.8 ± 0.7
ISO				
3.6	"P1_3p6_UM"	1.00	90	0.060 ± 0.018
4.8	"P1_4p8_UM"	1.53	90	0.53 ± 0.11
10.0	"P1_10_UM"	1.80	90	14.27 ± 2.8
12.8	"P1_12p8_UM"	2.40	90	24.97 ± 5.0
21.0	"P2_20_UM"	9.03	90	32.48 ± 6.5
23.8	"P2_25_UM"	9.12	90	32.69 ± 6.5
60.9	"P3_60_UM"	25.9	90	15.58 ± 4.7
102.4	"P3_100_UM"	39.5	90	3.91 ± 1.2
HST				
0.723	"28X50LP"	0.200	0.5	$(2.6 \pm 0.2) \times 10^{-4}$ [c]

Table 5.2 – Notes

[a] Width at half-maximum efficiency for ESO (Käufl 1997) and *HST* (Space Telescope Science Institute 1998). For *ISO*, the width of the equivalent rectangular filter that has a height of the mean efficiency of the real filter (Klaas *et al.* 1994, Laureijs *et al.* 1998).
[b] Fluxes refer to the comet's brightness at a geocentric distance of 0.32 AU and in the middle of the amplitude due to rotation.
[c] Flux is valid for $\lambda = 0.64$ μ, i.e., Cousins R band. We transformed the instrumental flux to this band. The equivalent magnitude is 17.7 ± 0.1.

effective on-source integration time is 47.5 min. Figure 5.2a compares this median comet's and α Cen A's enclosed flux as a function of photocentric distance. The star is a proxy for the PSF, taken during the course of the 61 comet images. The graph shows that a higher fraction of the comet's flux resides in the wings compared to the PSF, and hence the comet is an extended source, although the extent may be an artifact of imprecise adding of the images. The amount of coma in the image is calculated in Section 5.3.2.

Figure 5.3 shows our time series of the comet's flux over four nights. The flux and 1-σ error bar of each point are calculated from three flux measurements spaced closely in time. The time axis is modulo 15.2 hr to show the periodicity in the data (explained in Section 5.4.1). The ordinate is heliocentric magnitude m_h at a wavelength of 10.7 μm, which is related to the observed apparent magnitude m by

$$m_h = m - 5\log\left(\frac{\Delta}{1\mathrm{AU}}\right), \tag{5.1}$$

where Δ is the geocentric distance. This accounts for the changes in brightness due to the rapidly varying Δ during the observing run. The 10.7-μm flux of the comet, referred to the geocentric distance on 1997 Jul 19.0 UT ($\Delta = 0.32$ AU), and midway between the minimum and maximum flux of the rotational variation, was 3.1 ± 0.2 Jy.

5.3.2 *ISO* Photometry

The high spatial resolution of the ESO image has resolved out most of the comatic flux, but it is clear from Table 5.2 that Comet Encke had a dust coma: the flux measured with *ISOPHOT* in the $\sim$11 μm range is much higher than that measured with TIMMI. Using the aperture size ($\rho_{\mathrm{ISO}} = 90''$) and flux, we can estimate the amount of coma in the ESO image (Fig. 5.1a), as follows. Let F_{ESO} be the flux measured from the comet via our ground-based imaging, 3.1 ± 0.2 Jy. The aperture radius ρ_{ESO} is $3''$. Let F_{ISO} be the flux measured by *ISO* within its aperture. The wavelengths sampled by ESO and *ISO* do not exactly match but interpolating with a cubic spline we find that *ISO* saw 15$\pm$3 Jy at 10.7 μm. The rotational phase at the time of the *ISO* observations falls near a time of mid-brightness in the nucleus' rotation, though this is a small effect since the coma's flux dominates.

The flux measured at ESO is valid for heliocentric distance $r = 1.22$ AU, $\Delta = 0.32$ AU, and phase angle $\alpha = 44^\circ$, while the flux measured by *ISO* is valid for $r = 1.164$ AU, $\Delta = 0.263$, and $\alpha = 50.4^\circ$. To compare, we must correct for the geometry and apertures. First, we assume that the surface brightness of the coma is proportional to $1/\rho^n$, where ρ is the cometocentric distance, so that the comatic flux is proportional to $1/\Delta^n$, and that the flux within an aperture of radius of ρ_0 is proportional to ρ_0^{2-n}. A 12-μm ISOCAM image of the comet taken in early July 1997 (Reach *et al.* 1999) shows a coma with mean $n = 1.1$. Second, we assume that the comatic and nuclear fluxes are proportional to

$$\frac{1}{-1 + \exp\left(\frac{hc\sqrt{r}}{\lambda k T_0}\right)}, \tag{5.2}$$

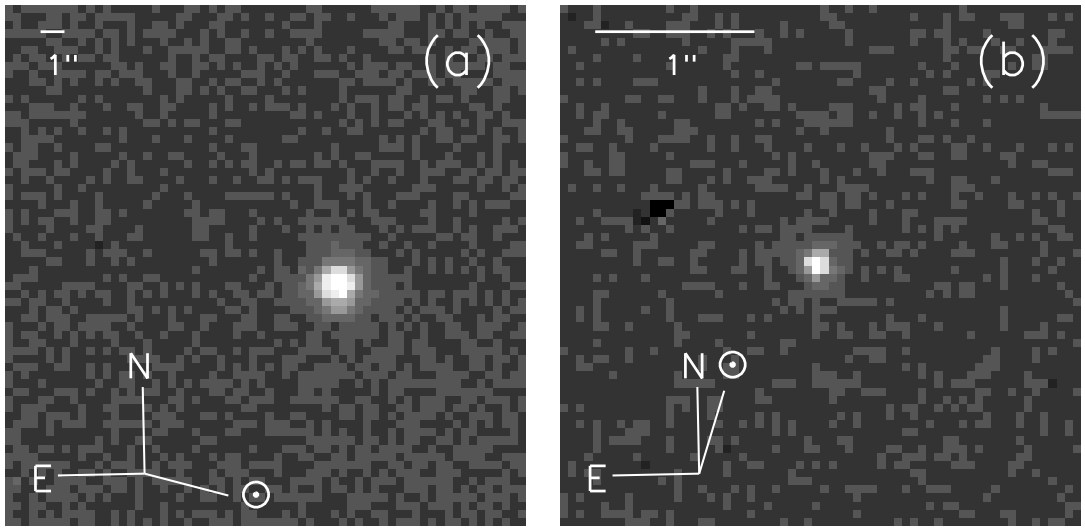

Figure 5.1: Comet Encke at 10 microns (a) and 7200 Angstroms (b). Here images of Comet 2P/Encke, with linear intensity scale, are displayed. Image (a) was taken with the TIMMI camera at ESO 3.6-m telescope on UT 18-19 Jul 1997, and image (b) was taken with the STIS instrument aboard *HST* on 1 Jul 1997. North, east, and the solar directions are marked. Pixel scales are $0.34''$ and $0.051''$, respectively. Wavelengths of observation are 10.7μm and 7200 Å, respectively. The ESO image is the weighted median of 61 individual frames, and the total integration time was 47.5 minutes. The *HST* image exposure time was 5 s.

where h is Planck's constant, c is the speed of light, k is Boltzmann's constant, and T_0 is 278 K $\sqrt{\text{AU}}$ for the coma and 331 K $\sqrt{\text{AU}}$ for the nucleus. This is just the representation for a sphere's and a hemisphere's, respectively, temperature. Since the two r are not very far apart this gross approximation will suffice. Third, we assume that the nuclear flux is proportional to $1/\Delta^2$ and $10^{-0.4\beta\alpha}$, where β is 0.011 mag/degree (further discussed in Section 5.4.4). Fourth, we assume no phase dependence over the phase angles for the thermal emission of the dust.

With these assumptions we calculate that *ISO* would have seen a coma that was $G_C = 1.41$ times brighter than what ESO saw with the same aperture, and a nucleus that was $G_N = 1.54$ times brighter. The aperture correction is $A = 21.35$. Let F_C and F_N be the flux of the coma and nucleus, respectively, as seen by ESO: $F_{\text{ESO}} = F_C + F_N$. Then $F_{\text{ISO}} = F_C G_C A + F_N G_N$. Solving, we find $F_N = 2.74 \pm 0.24$ Jy, $F_C = 0.36 \pm 0.11$ Jy, and thus only twelve percent of the flux seen by ESO is due to coma.

5.3.3 *HST* Photometry

Due to guide-star acquisition problems, only two images of the comet were acquired with STIS. Figure 5.1b shows the higher signal-to-noise image of the two, with a linear intensity scale. The integration time is only five seconds, which prevents us from seeing much of the extended structure. In addition, the high spatial resolution has resolved out most of the coma, Figure 5.2b compares the comet's and PSF's enclosed flux as a function of photocentric distance. The graph shows that a higher fraction of the comet's flux resides in the wings compared to the PSF, so the comet is an extended source. Also plotted is the profile of a model comet, with a point source nucleus plus a PSF-convolved $1/\rho$ coma, that mimics the real comet. About 75% to 85% of the flux is due to the nucleus, so in our analysis below we have assumed that the nucleus' magnitude is $-2.5\log(0.75) = 0.3$ mag fainter than the total magnitude. Fortunately the derivation of the absolute zero-phase magnitude (in Section 5.4.3) is insensitive to the exact *HST* magnitude within a few tenths.

5.4 Discussion

5.4.1 Periodicity of Flux.

We determined the aforementioned 15.2-hr periodicity in our ESO data using the string-length method outlined by Dworetsky (1983) mentioned in Chapter 3. The string length trials are shown in Fig. 5.4. Also marked in the figure are the possible periods quoted by Jewitt and Meech (1987; JM87 hereafter) and Luu and Jewitt (1990; LJ90 hereafter) using optical measurements near aphelion; there is good agreement among the three datasets. A 7.6-hr or 11.5-hr period gives a single-peaked light curve, but 15.2±0.3 hr, 22.4±0.8 hr, and the higher periods either imply two peaks or leave enough unsampled room in the phase plot to allow for a second peak and valley. One expects a double-peaked curve for a rotating nucleus as it shows different cross sections to the observer. The 15.2-hr period is the only one that gives temporal coverage of most of the rotational phase and shows two peaks.

The errors attached to the rotation periods are derived from a visual inspection of the phased light curve plot. Periods near the local minima in Fig. 5.4 are

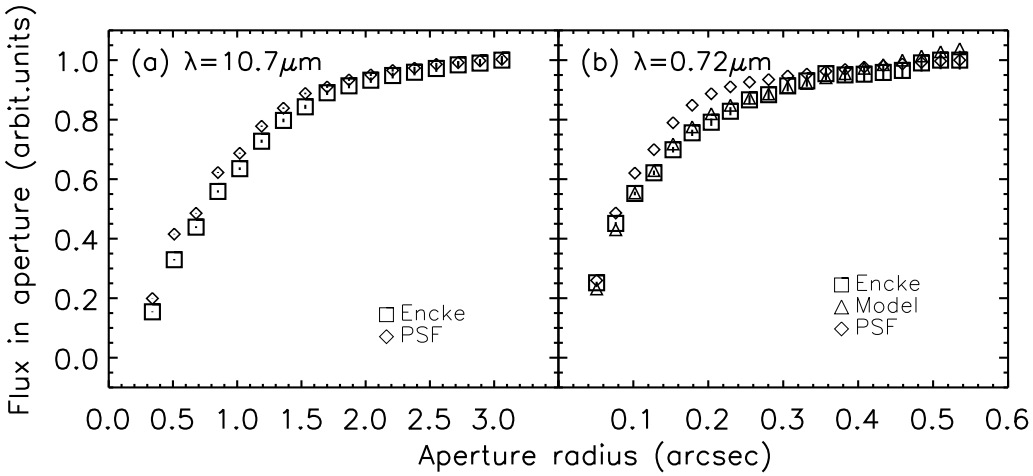

Figure 5.2: Radial profiles of Comet Encke in mid-IR (a) and optical (b). Here I compare the cumulative flux profiles of Comet Encke and the point-spread function. Squares are for the comet, diamonds are for the PSF, and triangles are for the model. (a) This is the profile from the TIMMI image in Fig. 5.1a. An image of α Cen A is used as a PSF proxy, and the profile is scaled to the right-most comet point. (b) This is a profile from the STIS image in Fig. 5.1b. A bright star imaged near in time with the same instrument setup is used as a PSF proxy, and the profile is scaled to the right-most comet point. The model is a point-source plus a PSF-convolved $1/\rho$ coma; the coma contributes 15% to 25% of the total flux.

acceptable only if the overlapping data in the phased light curve do not have widely disparate magnitudes. This defines the range of possible periods, and thus the errors are not normally distributed.

LJ90 remark that 15.08 ± 0.08 hr is "the most likely synodic period" of the nucleus' rotation, so our measurement is consistent with this. The correction from our measured synodic period to the sidereal period is small, since the aspect angle of the comet as seen by Earth changed by only about 0.6° per rotation period between UT 16.0 Jul and UT 22.0 Jul 1997. At most the correction is $0.6^\circ/360^\circ = 0.2\%$, much smaller than the fractional error $0.3/15.2 = 2\%$.

5.4.2 Shape and Precession of the Nucleus.

By inspection of Fig. 5.3, the peak-to-peak amplitude (p.t.p.a.) is 0.7 ± 0.1 mag, though it may be higher since we have not sampled all turnover points. This p.t.p.a. is similar both to that found for other comets (Meech 1999) and to that measured for Encke by JM87 and LJ90 in the optical regime. This variability is likely due to the changing cross section and not the albedo. The emissivity would have to be near 0.5 or 0.75, much too low, to explain this mid-IR variability with albedo spots, since the mid-IR flux is proportional to the emissivity.

Assuming that the results of JM87 and LJ90 and our ESO results are all free of coma contamination, we can constrain the nucleus' shape and rotation state. The four data points for this exercise are the different p.t.p.a.: JM87 measured the p.t.p.a. ≥ 0.8 mag on 23 Sep 1985, and ≥ 0.4 mag on 30 Oct 1986; LJ90 measured 0.62 ± 0.04 mag on 7 Sep 1988; and we measured ≥ 0.7 mag on 19 Jul 1997.

Sekanina (1988a) found a rotation axis direction that did not change much from 1924 to 1984, but this direction cannot account for the four p.t.p.a. – a drifting axis is required. We created a simple model where the angular momentum vector, initially at the location found by Sekanina (1988a), is pushed by a torque from the outgassing regions on the surface. The nucleus would be a triaxial ellipsoid in principal axis rotation about the shortest axis. To make the problem tractable we restricted this "precession" of the vector to a constant rate in a circle. The model thus has five parameters: the latitude and longitude of the precession axis, the period of the precession P_p, and the two axial ratios a/c and b/c of the nucleus (where c represents the short one). The p.t.p.a. δm is related to the shape by

$$\delta m = 1.25 \log\left(\frac{(a/c)^2 + \tan^2 l}{(b/c)^2 + \tan^2 l}\right), \tag{5.3}$$

where l is the sub-Earth latitude on the comet's surface.

With no degrees of freedom, we could find which parameter values were possible but not their likelihood. We found that (a) any precession axis direction greater than 14° from the angular momentum vector was allowable, (b) P_p must be ≤ 81 years, (c) a/c must be ≥ 2.6, and (d) $1.0 \leq b/c \leq 0.5 \times a/c - 0.3$. Furthermore the limit of P_p is smaller for smaller values of b/c. This short precession period and high elongation are necessary to reconcile the p.t.p.a. lower limits in 1985 and 1997 with the p.t.p.a. that was smaller in 1988.

Comparing with a review by Meech (1999), Encke's long axial ratio is toward the high end of known values, with four nuclei having a ratio of 2 or larger. Only

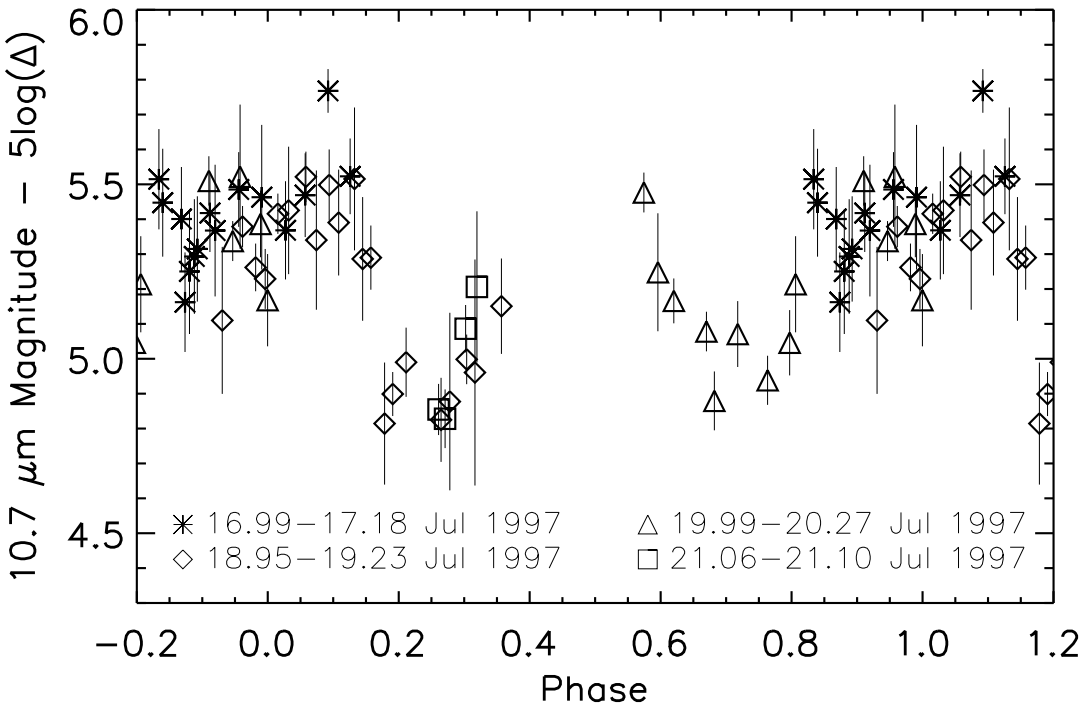

Figure 5.3: Light curve of Comet Encke phased by 15.2 hr. This is a four-day light curve of comet Encke, where the time coordinate is modulo 15.2 hr. The ordinate shows heliocentric magnitude in the 10.7-μm filter. The periodicity is derived from Fig. 5.4. Zero phase corresponds to 1997 Jul 19.0 UT.

29P/Schwassmann-Wachmann 1 has a ratio as large as 2.6. However many of these are projected ratios so it is unclear how Encke precisely compares to these other bodies. A recent study of comet 19P/Borrelly's nucleus yielded a deprojected axial ratio of 2.4 (Lamy *et al.* 1998b).

According to Sekanina's analysis (1988a,b), the comet's angular momentum vector was precessing at a continuously decreasing rate (averaging 0.3°/yr) until around 1924, after which it was mostly constant up to 1984. A mass ejection event or the activation of new vents may have occurred in the mid-1980s to start the nucleus precessing again. Although Samarasinha and Belton (1995) showed that the nucleus' ratio of precession to rotation period could evolve to a constant value, that assumes a consistent pattern of outgassing orbit after orbit, which may not be the case for Encke. Samarasinha and Belton (1995) and Samarasinha (1997) also mention that the nucleus will spin up and eventually orient itself with the pole pointing at the orbital longitude at which maximum outgassing occurs. (Usually this is just the Sun's cometocentric longitude at the comet's perihelion.) The uncertainties here are too great to address this; the *CONTOUR* visit in 2003 will hopefully help our understanding of Encke's rotation state.

The contribution of the coma to the rotational modulation is important to consider. If coma was present in JM87's and LJ90's photometry but not rotationally modulated then the lower limits to the p.t.p.a. are even higher and the limits on P_p, a/c, and b/c would be more extreme. If however the coma was modulated by e.g. an active patch or small jet swinging in and out of view, then the comet's light curve would show the addition of two oscillating curves – a two-peak curve from the nucleus and a one-peak curve from the coma – and the nuclear p.t.p.a. could be smaller than the total p.t.p.a. We argue here though that the comatic contribution to the amplitude is probably negligible. First, the bright aphelion outburst witnessed by Barker *et al.* (1981) showed no extended emission but completely obliterated any modulation of the flux over the course of the night. Hence we suppose that the coma's flux in the outburst was not tied to its natal active area. Second, LJ90 show no difference between the amplitudes and shapes of their light curve's two peaks, unlike what one would expect if there were a strong, singly-peaked, comainduced underlying curve.

Our own light curve (Fig. 5.3) may be asymmetric between the two peaks but the photometric uncertainties are too large to be sure. A lower 1997 p.t.p.a. than the one used above would slightly mitigate the axial ratio and precession period limits, but the optical data of JM87 and LJ90 are the more restrictive constraints.

5.4.3 Optical Phase Behavior.

We combined our *HST* nuclear magnitude with measurements from previous apparitions to estimate the phase behavior of the nucleus and derive the absolute magnitude $m(1,1,0)$. We used three phase laws: the linear law

$$m(1,1,\alpha) = m(1,1,0) + \beta\alpha, \tag{5.4}$$

where β is a constant; the IAU-adopted (H,G) formalism for asteroids (Lumme *et*

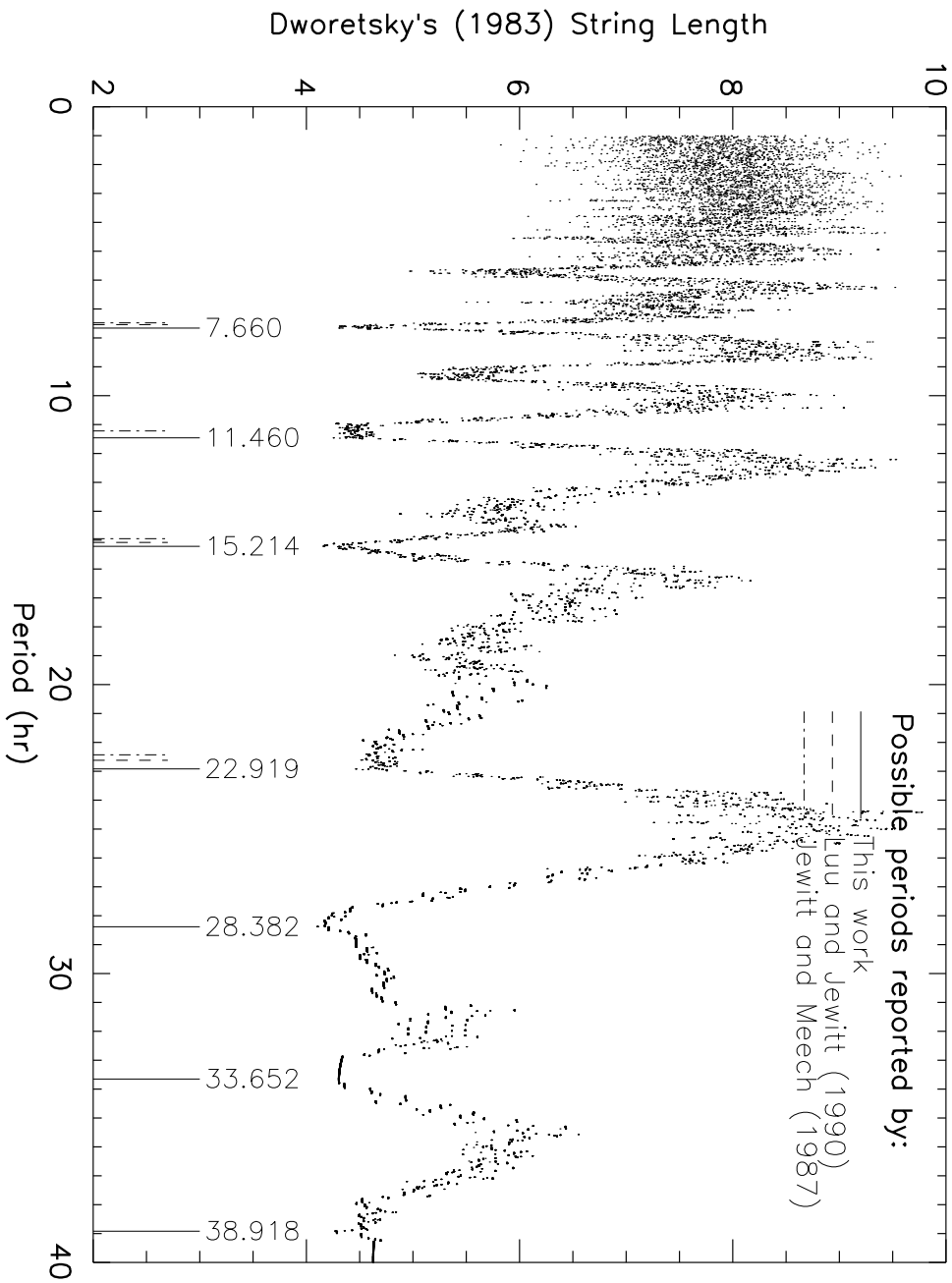

Figure 5.4: String-length method determination of Encke's rotation period. This is a diagram to find periodcity based on the method of Dworetsky (1983). Four days' worth of data were used to find the rotation period. Minima indicate the most likely rotation periods, but some are more favorable than others; text gives details. The dashed and dash-dotted lines indicate periods that have been postulated by LJ90 and JM87.

al. 1984, Swings 1985)

$$m(1,1,\alpha) = H - 2.5\log\Big[(1-G)e^{-3.33\tan^{0.63}(\alpha/2)} + Ge^{-1.87\tan^{1.22}(\alpha/2)}\Big], \quad (5.5)$$

where $H = m(1,1,0)$; and the original Lumme-Bowell law (Lumme and Bowell 1981):

$$m(1,1,\alpha) = m(1,1,0) - 2.5\log F, \quad (5.6)$$
$$F \equiv (1-Q)e^{-3.343\tan^{0.632}(\alpha/2)} + (Q/\pi)(\sin\alpha + (\pi-\alpha)\cos\alpha),$$

where Q is the fraction of multiply-scattered light.

Figure 5.5 shows a plot of $m(1,1,\alpha)$ for the Encke nucleus as measured by several observers; the data with notes are listed in Table 5.3. An observer had to report either the "nuclear" magnitude or the "m_2" magnitude to have his/her datum included in this plot. The ordinate $m(1,1,\alpha)$ is the observed magnitude minus the geometric factor $5\log(r\Delta)$. Symbols indicate some information about each datum, written in the legend. The data from LJ90, JM87, Barker *et al.* (1981), Garradd (1997), Spinrad (as reported by LJ90), and us were taken with linear-response detectors; the other points are photographic. Our data and those of Garradd (1997) do not have much coma contamination despite being taken at low r. Of the historical data, only JM87, LJ90, and Barker *et al.* (1981) have information on the rotation of the nucleus, hence all the other points have an uncertainty of at least ± 0.4 mag, i.e., half the approximate p.t.p.a. Only Barker *et al.* (1981) and LJ90 were able to measure enough of the light curve to factor out the rotational modulation; in the former case there was no modulation detected. JM87 were twice able to find the turnover point at the bright end of the rotational variation, but not at the dim end, so we have used magnitudes for Fig. 5.5 that (we estimate) probably lie close to the average brightness and we have assigned sensible error bars. (Specifically, for one point we plotted a magnitude 0.6 mag fainter than their extremum, with errors of ± 0.2 mag; for the other point, we plotted a magnitude 0.4 mag fainter than their extremum, with errors of ± 0.3 mag.)

We assigned a photometric error of ± 0.5 mag to photographic data. This partially comes from the fact that Roemer and Lloyd (1966) photographed the comet only 14 minutes after van Biesbroeck (1962) did on 22 Oct 1960 and yet they differ in their magnitude estimates by 0.9 mag. Combined with the 0.4 mag of uncertainty due to rotation the total error is about 0.6 mag. We assigned an error of 0.1 mag to the data from linear-response detectors when no other estimate was available. Thus, the rotational uncertainty dominates, and the total uncertainty is about 0.4 mag.

We converted all data in Table 5.3 to Cousins R magnitude R_C, the band of our *HST* magnitude, before plotting in Fig. 5.5. To do this we assumed the following solar colors: (a) $B_J - R_J = 1.17$ (Allen 1973), (b) $B_J - m_{pg} = 0.11$ (Allen 1973), (c) $V_J - m_{pv} = 0.0$ (Allen 1973), (d) $V_J - R_J = 0.52$ (Allen 1973), (e) $R_J - R_C = -0.17$ (Fernie 1983), and (f) $R_{Mould} - R_C = -0.17$. For some points (noted in Table 5.3) we have assumed that the photographic data were taken on blue plates so that m_{pg} is the applicable quantity. (Roemer [1965] for example explicitly states that this is the case.)

Figure 5.5 (next page): Optical phase behavior of comet Encke's nucleus. By collecting historical data, I plot comet Encke's nuclear magnitude as a function of phase angle. Ordinate is in Cousins R magnitude, offset by $-5\log(r\Delta)$ to account for differing observing geometries. A linear phase law, the Lumme-Bowell (Lumme and Bowell 1981) phase law, and the IAU-style asteroid phase law (Lumme *et al.* 1984, Swings 1985) are plotted. Despite the uncertain interpretation of some reported magnitudes, there is steep phase darkening, more drastic than that of other cometary nuclei and C type asteroids (shown).

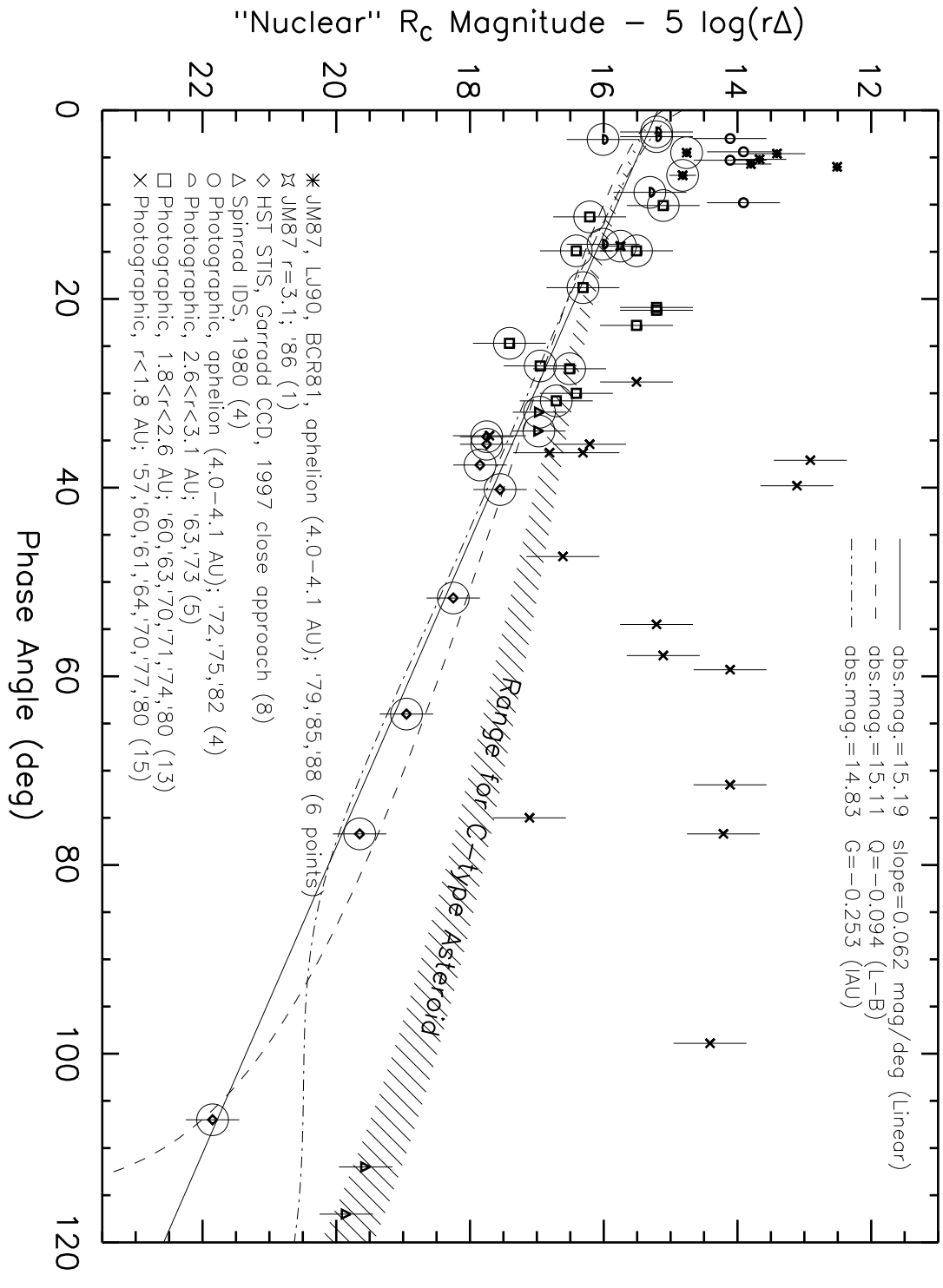
"Nuclear" R_c Magnitude − 5 log(rΔ)
Phase Angle (deg)
abs.mag.=15.19 slope=0.062 mag/deg (Linear)
abs.mag.=15.11 Q=−0.094 (L−B)
abs.mag.=14.83 G=−0.253 (IAU)
Range for C-type Asteroid
✳ JM87, LJ90, BCR81, aphelion (4.0−4.1 AU); '79,'85,'88 (6 points)
⧆ JM87 r=3.1; '86 (1)
◇ HST STIS, Garradd CCD, 1997 close approach (8)
△ Spinrad IDS, 1980 (4)
○ Photographic, aphelion (4.0−4.1 AU); '72,'75,'82 (4)
⊃ Photographic, 2.6<r<3.1 AU; '63,'73 (5)
□ Photographic, 1.8<r<2.6 AU; '60,'63,'70,'71,'74,'80 (13)
× Photographic, r<1.8 AU; '57,'60,'61,'64,'70,'77,'80 (15)

Table 5.3. Estimated "Nuclear" or "m_2" Magnitudes for Encke's Nucleus

Date (UT)	Medium[a]	Band[b]	Reported Mag.	α (°)	r[c] (AU)	Δ (AU)	Color Crxn.[d]	$m(1,1,\alpha)$ [e]	Coma? [f]	Wt. [g]	Ref. [k]
30.5 Jul 1997	CCD	V_J	17.4	34.6	1.39	0.51	-0.35	17.8	F	2	1
28.5 Jul 1997	CCD	V_J	17.1	35.4	1.36	0.47	-0.35	17.7	F	2	1
24.5 Jul 1997	CCD	V_J	16.9	37.6	1.31	0.41	-0.35	17.9	F	2	1
21.4 Jul 1997	CCD	V_J	16.2	40.2	1.26	0.36	-0.35	17.6	F	1	1
14.4 Jul 1997	CCD	V_J	16.0	51.7	1.16	0.26	-0.35	18.3	F	2	1
10.5 Jul 1997	CCD	V_J	16.1	64.0	1.09	0.21	-0.35	19.7	F	2	1
7.4 Jul 1997	CCD	V_J	16.6	76.7	1.04	0.20	-0.35	20.0	F	2	1
1.3 Jul 1997	CCD	R_C	17.92	106	0.94	0.20	0.0	21.85[h]	F	2	2
3-7 Sep 1988	CCD	R_M	19.8	4.2	3.83	2.85	+0.17	14.76	N	1	3
30 Oct-3 Nov 1986	CCD	R_M	20.0[i]	14.8	3.15	2.46	+0.17	15.75	N	1	4
22-23 Sep 1985	CCD	R_M	20.2[j]	6.8	4.06	3.15	+0.17	14.82	N	1	4
30 Jul 1982	Photo	m_{pg}*	20.5	9.8	4.10	3.3	-0.89	13.9	?	0	5
5 Nov 1980	IDS	R_M	16.7	117	0.82	0.31	+0.17	19.9	Y	0	7

Table 5.3 – continued

Date (UT)	Medium[a]	Band[b]	Reported Mag.	α (°)	r^c (AU)	Δ (AU)	Color Crxn.[d]	$m(1,1,\alpha)$ [e]	Coma? [f]	Wt. [g]	Ref. [k]
4 Nov 1980	IDS	R_M	16.5	112	0.84	0.31	+0.17	19.6	Y	0	7
8 Oct 1980	Photo	m_{pg}*	16.5	47.3	1.26	0.49	-0.89	16.6	Y	0	6
7 Sep 1980	IDS	R_M	18.1	34	1.69	1.09	+0.17	17.0	Y	1	7
21 Aug 1980	IDS	R_M	19.0	32	1.90	1.47	+0.17	17.0	Y	1	7
13 Aug 1980	Photo	m_{pg}*	20.0	30.8	1.80	1.65	-0.89	16.7	?	1	8
8.5 Aug 1980	Photo	m_{pg}*	20	30.0	2.02	1.75	-0.89	16.4	?	0	9
26 Aug 1979	DAP	V_J	19.13	4.6	3.96	2.99	-0.35	13.21	N	0	10
24 Aug 1979	DAP	V_J	19.39	5.2	3.96	3.00	-0.35	13.67	N	0	10
22 Aug 1979	DAP	V_J	19.53	5.7	3.96	3.01	-0.35	13.80	N	0	10
21 Aug 1979	DAP	V_J	18.25	6.0	3.97	3.02	-0.35	12.51	N	0	10
14.3 Oct 1977	Photo	m_{pg}*	15.1	39.8	1.17	1.56	-0.89	12.9	?	0	11
9.3 Oct 1977	Photo	m_{pg}*	15.6	37.1	1.25	1.65	-0.89	13.1	?	0	11
12 Sep 1975	Photo	m_{pg}	20.2	4.4	4.02	3.05	-0.89	13.9	N	0	12

Table 5.3 – continued

Date (UT)	Medium[a]	Band[b]	Reported Mag.	α (°)	r[c] (AU)	Δ (AU)	Color Crxn.[d]	$m(1,1,\alpha)$ [e]	Coma? [f]	Wt. [g]	Ref. [k]
12 Sep 1974	Photo	m_{pg}	21.0	24.7	2.19	1.58	-0.89	17.4	?	2	13
25.0 Oct 1973	Photo	m_{pg}*	20.25	14.2	2.63	1.80	-0.89	16.0	?	2	15
26 Sep 1973	Photo	m_{pg}	20.5	3.1	2.85	1.86	-0.89	16.0	N	2	14
13 Sep 1972	Photo	m_{pg}	20.5	3.0	4.09	3.11	-0.89	14.1	N	0	16
15 Aug 1972	Photo	m_{pg}	20.5	5.3	4.09	3.13	-0.89	14.1	N	0	16
29 May 1971	Photo	m_{pv}	20.5	27.1	2.22	1.95	-0.35	16.9	N	2	17
27 May 1971	Photo	m_{pg}	20.6	27.4	2.20	1.97	-0.89	16.5	N	1	17
28 Nov 1970	Photo	m_{pg}	16.5	75.0	1.00	0.43	-0.89	17.1	Y	0	18
26.4 Sep 1970	Photo	m_{pg}	18.4	18.8	1.87	0.95	-0.89	16.3	Y	2	18
7.1 Sep 1964	Photo	m_{pg}	18.6	34.5	1.75	1.26	-0.89	16.0	Y	0	19
30.2 Aug 1964	Photo	m_{pg}	19.0	36.3	1.65	1.08	-0.89	16.8	Y	0	19
16.1 Dec 1963	Photo	m_{pg}	20.3	22.8	2.50	2.46	-0.89	15.5	N	0	19
12.3 Oct 1963	Photo	m_{pg}	20.2	8.7	2.99	2.07	-0.89	15.3	N	1	19

Table 5.3 – continued

Date (UT)	Medium[a]	Band[b]	Reported Mag.	α (°)	r[c] (AU)	Δ (AU)	Color Crxn.[d]	$m(1,1,\alpha)$ [e]	Coma? [f]	Wt. [g]	Ref. [k]
25.4 Sep 1963	Photo	m_{pg}	20.2	2.6	3.10	2.11	-0.89	15.2	N	1	19
24.3 Sep 1963	Photo	m_{pg}	20.2	2.5	3.11	2.11	-0.89	15.2	N	1	19
17.1 Jan 1961	Photo	m_{pg}	14.3	98.9	0.59	0.70	-0.89	14.4	Y	0	19
6.1 Jan 1961	Photo	m_{pg}	15.0	76.7	0.79	0.79	-0.89	14.2	Y	0	19
20.2 Dec 1960	Photo	m_{pg}	17.0	59.3	1.08	0.87	-0.89	14.1	Y	0	19
8.2 Nov 1960	Photo	m_{pg}	15.9	28.8	1.67	0.89	-0.89	15.5	N	0	19
22.1 Oct 1960	Photo	m_{pg}	17.6	14.9	1.87	0.94	-0.89	15.5	N	1	19
22.1 Oct 1960	Photo	m_{pg}	18.5	14.9	1.87	0.94	-0.89	16.4	F	2	21
17.3 Oct 1960	Photo	m_{pg}	18.5	11.3	1.93	0.97	-0.89	16.2	F	2	21
26.2 Sep 1960	Photo	m_{pg}	18.0	10.1	2.15	1.19	-0.89	15.1	N	1	19
19.3 Aug 1960	Photo	m_{pg}	19.5	20.9	2.51	1.87	-0.89	15.2	N	0	19
17.3 Aug 1960	Photo	m_{pg}	19.5	21.2	2.52	1.91	-0.89	15.2	N	0	19
19.4 Sep 1957	Photo	m_{pg}	15	71.5	0.80	0.91	-0.89	14.8	Y	0	20

Table 5.3 – continued

Date (UT)	Medium[a]	Band[b]	Reported Mag.	α (°)	r[c] (AU)	Δ (AU)	Color Crxn.[d]	$m(1,1,\alpha)$ [e]	Coma? [f]	Wt. [g]	Ref. [k]
4.4 Sep 1957	Photo	m_{pg}	16	57.8	1.05	1.03	-0.89	14.9	Y	0	20
31.4 Aug 1957	Photo	m_{pg}	16.5	54.5	1.12	1.08	-0.89	15.2	Y	0	20
30.4 Jul 1957	Photo	m_{pg}	19.3	36.3	1.57	1.67	-0.89	16.3	Y	0	20
28.4 Jul 1957	Photo	m_{pg}	19.3	35.4	1.60	1.72	-0.89	16.2	Y	0	20

[a] CCD = Charge-coupled device. Photo = photographic plates. IDS = image dissector scanner. DAP = digital area photometer.

[b] Asterisks indicate where the use of a blue-sensitive plate was assumed.

[c] Aphelion: $r = 4.1$ AU; Perihelion: $r = 0.3$ AU.

[d] Term to convert from reported magnitude to R_C band.

[e] $m(1,1,\alpha)$ = Reported Mag. $-5\log(r\Delta)$ + Color Crxn.

[f] Indicates presence of an observed coma: Y = yes, F = yes but faint, N = no, ? = unknown.

[g] Relative weight of the point used when fitting the phase law.

Table 5.3 – continued

[h] Added 0.3 mag to account for coma.

[i] Magnitude is 0.4 mag fainter than authors' reported bright extremum.

[j] Magnitude is 0.6 mag fainter than authors' reported bright extremum.

[k] References: 1 = Garradd 1997. 2 = This work. 3 = LJ90. 4 = JM87. 5 = Gibson, reported by Marsden 1985b. 6 = Shao and Schwartz 1980. 7 = Spinrad 1985, private communication reported in JM87. 8 = Shao, reported by Marsden 1985a. 9 = Helin *et al.* 1980. 10 = Barker *et al.* 1981. 11 = Gilmore and Kilmartin 1978. 12 = Roemer, reported by Marsden and Roemer 1978b. 13 = Roemer, reported by Marsden and Roemer 1978a. 14 = Roemer, reported by Marsden 1974. 15 = Shao 1973. 16 = Roemer, reported by Marsden 1973. 17 = Roemer, reported by Marsden 1972. 18 = Roemer, reported by Marsden 1971. 19 = Roemer and Lloyd 1966. 20 = Roemer 1965. 21 = van Biesbroeck 1962.

Ideally all the points would tightly follow a curve, but clearly some choice has to be made about which data are worth fitting, since the coma contamination is obvious for some points, e.g. the ten photographic points at low r between $35^\circ < \alpha < 100^\circ$. For such points the observers likely measured the comet's central condensation (inner coma) rather than the nucleus itself. With other points the exact amount of contamination is unclear, it may be none or half a magnitude's worth. An indication of how much coma contamination there is might be determined by looking at the intrinsically faintest data at a given α, but in this case that is not so helpful because that usually turns out to be a photographic point and the error bars are too large. Hence, it is nontrivial to incorporate all the data into a fit to the phase law. Moreover the problem is most contentious at low phase angle, i.e., right at the location where we need the best data to determine the absolute magnitude. The data point due to LJ90 is very well determined (± 0.04 mag), and so normally would provide a very good constraint; however, if there were a tiny amount of coma contamination, that would compromise its usefulness in the fitting.

A further complication is that the plotted error bars are not normally distributed, so any fit statistic must be carefully interpreted. A sinusoidally-varying flux spends more time at the extrema than at the average value, so the measured value is likely to be far from the average brightness.

Our solution is to fit the phase laws through the selection of points marked in Table 5.3 and enclosed in circles in Fig. 5.5. We use all of the linear-detector data and the fainter photographic points. For a given point we assigned it double weight if it was an intrinsically fainter point relative to its immediate neighbors in phase angle. The results are provided in Fig. 5.5. The r.m.s. offset is about 0.4 mag for all three fits. The IAU law fails at the higher phase angle but the other two laws are adequate. Considering the uncertainties we take the absolute magnitude to be 15.2 ± 0.5 mag.

The slope of the phase law is quite steep at 0.06 mag/degree, making Encke's nucleus one of the most phase-darkened objects in the Solar System. It is possible that shape effects are anomalously depressing the brightness at high phase angle and fooling us, but the smooth, linear behavior of our *HST* point and the Garradd (1997) points argue against this. Cometary nuclei (Jewitt and Meech 1988, Chapter 7 of this thesis) and C-type asteroids (Lumme and Bowell 1981), to which the nuclei are commonly thought to be evolutionarily linked, typically have only about 0.04 mag/degree of phase effect, as drawn in Fig. 5.5. Further study of the phase behavior of near-Earth asteroids (NEAs) and cometary nuclei over a large range of α is clearly desirable.

The unphysical and negative value of Q, the fraction of multiply scattered light, and the steep slope both imply that the surface of Encke is very rough. Lumme and Bowell (1981) mention this phenomenon in reference to (944) Hidalgo, a cometary candidate also with $Q < 0$. Specifically, the depth-to-diameter ratio of features on the surface is apparently larger than for their average asteroid, and Q is actually close to zero. This makes sense since the reflectivity of the nucleus is so low, so very few measured photons would have been multiply scattered.

It is interesting to note that the aphelion data from 1972, 1975, 1979, and 1982 all apparently have significant coma, though none were spatially resolved by

the observers. The Barker *et al.* (1981) data prove that aphelion outbursts exist, and it is important to justify the inability to spatially resolve the coma, which we assume is mostly dust. Some measurements had fairly large seeing disks which could potentially hide the coma, but JM87 and LJ90, with $\sim 1''$ seeing, specifically used differing apertures to detect comatic flux, but did not find any. Thus, any existing dust would have to be slow-moving and/or have a surface brightness steeper than the usual dependence on cometocentric distance. We know that large (tens to thousands of microns) grains are emitted by Encke from *IRAS* trail and *ISO* tail and trail observations (Sykes and Walker 1992, Reach *et al.* 1999, Lisse *et al.* 2000), and such particles move slowly with respect to the nucleus since radiation pressure is inefficient. Thus, it is not unreasonable to expect that the outbursts originate as large dust grains traveling at $\sim$1 m/s (i.e., just below escape velocity) and eventually falling back on to the surface. At aphelion the largest dust grain that can be lifted off the nucleus has a radius of just 130 μm $\times$ $(\frac{v_g}{10\ \mathrm{m/s}})$ $\times$ $(Z \times 10^{-16}\mathrm{s\ cm^2})$, where v_g is the speed of the gas and Z is the vaporization rate, based on an equation given by Keller (1990).

5.4.4 Nucleus Size and Geometric Albedo.

Now we can apply the thermal model to the data. First, let us assume $\epsilon = 0.9$ and $T_{ss} = 360$ K (which will be justified below). If $\Gamma = 50$ J K^{-1} m^{-2} s$^{-1/2}$, i.e. about the lunar value (Winter and Saari 1969), then $\Theta = 0.23$ (defined in Chapter 3) and Encke's nucleus is a moderately slow-rotator. Harris *et al.* (1998) estimate $\Gamma = 320$ J K^{-1} m^{-2} s$^{-1/2}$ on the surface of (3200) Phaethon, which is presumably an extinct comet owing to its parentage of the Geminid meteor stream; if applicable to Encke's nucleus, $\Theta = 1.5$, placing it on the border between slow and fast rotator. Thus the STM will work reasonably well but not perfectly represent Encke's thermal behavior. Since the orientation of the nucleus' spin axis appears to have changed since the Sekanina (1988a) analysis, it would be difficult to constrain any of the other parameters in the augmented thermal model even though we have derived some information about the shape. Thus we will apply the STM and compare the results with the RRM to get some sense of the model-dependent error.

Some parameters of the STM were assumed to be as follows: infrared phase coefficient β_i, 0.005 to 0.017 mag/degree; emissivity ϵ, 0.9; optical phase integral q, 0.17, which can be derived from the phase analysis of a previous section; beaming parameter η, 0.7 to 1.2. For the RRM, we assume the limiting case of the rotation axis perpendicular to the Sun-Earth-Comet plane.

In Section 5.3.3 we found the nucleus' flux to be 2.74 ± 0.24 Jy; for this flux the STM provides us with an effective radius R_N of 2.40 ± 0.27 km and a subsolar temperature T_{SS} in mid-July 1997 of 365 ± 14 K. This justifies our use of 360 K in the Θ calculation above. The (1-σ) errors are derived from a Monte Carlo simulation letting $0.9 < \epsilon < 1.0$, $0.7 < \eta < 1.2$, and $0.005 < \beta_i < 0.017$, all uniformly distributed, and using the normally-distributed flux estimate. By similarly applying the simplified RRM, we find $R_N = 3.55 \pm 0.15$ km and $T_{SS} = 270 \pm 5$ K. These may be interpreted as the upper and lower limits, respectively, to these quantities since they would be physical only if we were grossly underestimating the thermal

inertia of cometary nuclei. It is clear however that if the thermal inertia is more Phaethon-like than Moon-like then R_N is probably a few tenths of a kilometer larger than that given by the STM.

From our discussion in Section 5.4.3 we estimate the optical cross section at zero phase angle to be equivalent to a magnitude of 15.2 ± 0.5. The relation between the optical cross section and the comet's magnitude is

$$pR_N^2 = 2.238 \times 10^{16} \text{ km}^2 \times 10^{0.4(m_\odot - m(1,1,0))} \tag{5.8}$$

based on an equation given by Jewitt (1991), where p is the geometric R band albedo and $m_\odot$ is the solar apparent R band magnitude of -27.10. We calculate from this that $p = 0.047 \pm 0.023$.

5.4.5 Consistency with *ISO* Data.

Our broadband spectrophotometry obtained by *ISO* is shown in Fig. 5.6. The dust's contribution to these data is more fully discussed in a related paper by Lisse *et al.* (2000). Presently we will only show that our other results are consistent with this dataset.

Our simple model of the spectrum uses the sum of two component spectra, one for the dust and one for the nucleus. Reach *et al.* (1999) have shown that there is a significant population of large (radius $\gtrsim 100$ μm) grains in Encke's coma, so we have modeled the thermal emission of the dust in the 4.8 to 100 μm wavelength range as a greybody, with temperature as a free parameter and emissivity independent of wavelength. Such a null dependence can explain mid-IR observations of large dust grains from other comets (Lisse *et al.* 1998). We are unconcerned with the actual values of the dust's emissivity and optical depth; we scale our model to yield the best fit for particular values of the parameters. ISOPHOT's 3.6 μm flux has a significant scattered sunlight component in addition to the thermal emission and so is not used to constrain our model beyond being an upper limit to the thermal flux.

We modeled the spectrum of the nucleus using the STM, choosing η to be either 0.7, 0.95, or 1.2, β_i to be either 0.005 or 0.017 mag/degree, and ϵ to be 0.9. The parameter R_N could be any value. Thus our model has four important parameters: temperature of the dust T_D, R_N, η, β_i. An example model and the excellent fit to the spectrophotometry are shown in Fig. 5.6.

With this methodology, the results of the fitting can be displayed as a contour plot of the reduced χ^2 fit-statistic (χ^2_ν) as a function of T_D and R_N. The six plots in Fig. 5.7 show this, for each value of η and β_i. Owing to the low number of spectrum points vis-à-vis the model parameters, it is impossible to constrain the four parameters, but the ISOPHOT spectrum is consistent with our ground-based derivation of R_N (whose 1-σ boundaries are noted by the shaded rectangles) across the range of previously-found values for η and β_i. In particular, η cannot be constrained from Fig. 5.7 since the ESO constraint on R_N never strays far from $\chi^2_\nu \approx 1$, even when $\eta = 0.7$. It is satisfying that the derived dust temperatures are sensible; an isothermal black body at Encke's distance from the Sun would have $T_D = 258$ K.

5.5 Previous Work

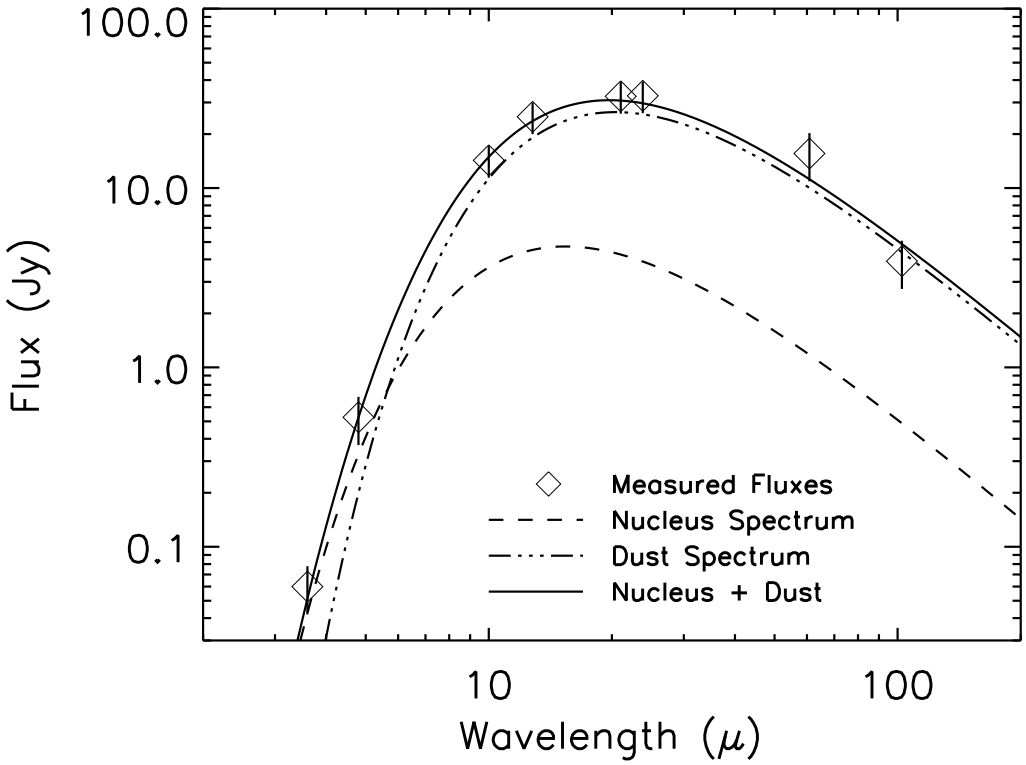

Figure 5.6: ISOPHOT spectrophotometry of Encke dust coma plus nucleus. The symbols show a broadband mid-infrared spectrum of the nucleus and dust of comet Encke, taken by ISOPHOT. Also plotted is a sample model (solid line) that fits the spectrum ($\chi^2_\nu = 0.64$ with 3 degrees of freedom, $R_N = 2.5$ km, $T_D = 250$ K, $\eta = 1.1$, $\beta_i = 0.01$ mag/degree). Dashed line is a model spectrum of the nucleus generated by the STM; dash-dotted line is a Planck spectrum of the dust.

Thermal infrared measurements in the past have been made by Ney (1974), Campins (1988), and Gehrz *et al.* (1989) to estimate the size of the nucleus. All used single-element bolometers, so no spatial information was obtained. The present study is an improvement because of our higher sensitivity and spatial resolution.

5.5.1 Ney (1974).

On 25 Apr 1974, Ney (1974) measured a flux of 11±1 and 19±2 Jy at wavelengths of 4.8 and 8.5 μm, respectively (converting from the reported magnitudes). His reported upper limit to Encke's R_N of 0.25 to 0.5 km is derived from an assumed correlation between nuclear size and comatic thermal infrared behavior, observations of Comet Bradfield (1974b = 1974 III = C/1974 C1), and an assumed value for the nuclear albedo that is now known to be too high. Instead, if we apply the STM to his Encke thermal fluxes, and use the assumptions we outlined in Section 5.4.4, we find an upper limit to the nuclear radius of approximately 7.5 km, which is above our calculated value.

5.5.2 Campins (1988).

Seven observations at 10.6 μm are reported during the 1984 apparition, two during the 1980 apparition, and the fluxes vary from 0.6 to 6.1 Jy. By using his intrinsically faintest data point, and applying the STM, he estimates an effective radius of $\leq$ 2.9 km at rotational minimum and $\leq$ 4.4 km at rotational maximum. These are the mid-IR measurements with formerly the least amount of coma contamination, but our calculated effective radius is smaller.

5.5.3 Gehrz *et al.* (1989).

Near and mid-IR measurements are reported on four dates during the 1974 apparition and two dates during the 1987 apparition, with fluxes ranging from 1 to 20 Jy. Using their intrinsically faintest data point, and assuming an isothermal nucleus (not the STM), they derive an upper limit to R_N of 5 km. Applying the STM to their reported fluxes gives an upper limit of 3 to 5 km, depending on the model's parameter values, which is above our calculated value.

5.5.4 Kamoun *et al.* (1982).

From the radar echoes at $\lambda = 12.6$ cm, these workers found a radar cross section of 1.1 ± 0.7 km^2 in the circular polarization sense orthogonal to that of the transmitted pulse. If Encke is like other comets where the radar's reflection is mostly specular (Harmon *et al.* 1989), then this is roughly the total radar cross section also. Further, using the bandwidth of the returned pulse, they found an effective radius R_N of $1.5^{+2.3}_{-1.0}$ km, although with more modern values of the rotation period (LJ90) and spin axis direction (Sekanina 1988a) R_N would be 4^{+6}_{-3} km. Our measurement of R_N is within this range.

With our effective radius in hand further rudimentary interpretation of the radar results are possible. The geometric albedo at $\lambda = 12.6$ cm, $p_{12.6}$, which is just

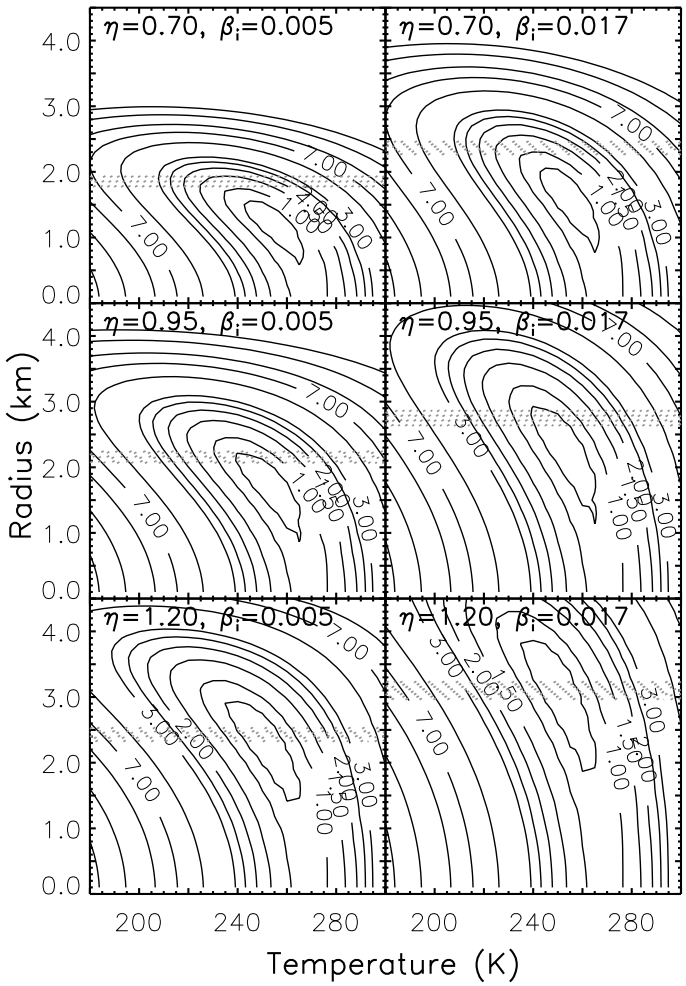

Figure 5.7: χ^2 plots of Encke dust temperature and nucleus size. Here are contour plots of χ^2_ν showing that the simple model described in the text – dust black body spectrum plus nucleus STM spectrum – adequately fits the *ISO* spectrum and is consistent with the ground-based results. Shaded rectangles indicate the 1-σ range of nuclear radii implied by our ESO data. Contour levels are 0.75, 1.0, 1.5, 2.0, 2.5, 3.0, 5.0, 7.0, 9.0, 12.0, and 15.0. Each panel represents one value of β_i and one value of η, leaving the other two parameters of the model – dust temperature and nuclear radius – to be plotted.

the radar cross section divided by πR_N^2, is 0.061 ± 0.041, a value comparable to the one at optical wavelengths and to that found for other comets (Harmon *et al.* 1989, Campbell *et al.* 1989). Following the argument and assumptions made by Harmon *et al.* (1989) in their treatment of Comet *IRAS*-Araki-Alcock (C/1983 H1), the dielectric constant of the Encke nucleus' surface layer is 2.3 ± 0.7, corresponding to (not surprisingly) a mixture of dust and snow.

5.6 Summary of Encke Results

We have discussed the properties of the nucleus of Comet 2P/Encke as derived from data obtained during its close approach to Earth in July 1997. The *CONTOUR* spacecraft is scheduled to encounter comet Encke in 2003 and this information can aid in the mission planning and design. We measured the thermal continuum of the comet in the 8 to 12 μm range with the TIMMI instrument at the ESO 3.6-m telescope and in the 3.6 to 100 μm range with the ISOPHOT photometer on the *ISO* spacecraft. We also used the STIS CCD aboard *HST* to measure the optical (5500-11000 Å) scattered continuum of the comet. We find the following:

• 1. Assuming the nucleus' thermal behavior can be described using the Standard Thermal Model (STM; Lebofsky and Spencer 1989), the effective nuclear radius is 2.4 km ± 0.3 km and the subsolar temperature at a distance of 1.2 AU from the Sun is 365 ± 14 K. The effective radius is smaller than the upper limits found by other researchers using thermal continuum observations (Ney 1974, Campins 1988, and Gehrz *et al.* 1989), and within the range found via the radar experiment in 1980 (Kamoun *et al.* 1982). The applicability of the STM could be questioned since the thermal inertia is unknown, but the effective radius is probably at most only a few tenths of a kilometer larger than the value given above.

• 2. Using our *HST* data and other datasets (JM87, LJ90, Garradd 1997) along with various photographic data from previous apparitions, we find the optical phase law of Encke's nucleus out to 106° can be well fit with a Lumme-Bowell phase law (Lumme and Bowell 1981) with absolute R_C band magnitude 15.2 ± 0.5 and $Q = -0.09$. The equivalent linear slope is 0.06 mag/degree, which is one of the steepest slopes known for any small body of the Solar System. The negative value of Q and the steep slope imply that the nucleus' surface is rougher than the typical asteroid used to create the Lumme-Bowell law. The absolute magnitude yields a visual geometric albedo for the nucleus of 0.05 ± 0.02. Use of this absolute magnitude does mean that bright (~ 1 mag) but spatially-unresolved outbursts were observed at several separate aphelia (4 AU) by many observers.

• 3. The nucleus' rotation period is likely 15.2 hr ± 0.3 hr, but our data cannot rule out some harmonics of this value, as they also show or imply a double-peaked light curve (i.e., as if we had observed a rotating nucleus). Optical measurements give 15.08 ± 0.08 hr (LJ90), so our data are consistent with this value.

• 4. We measured a peak-to-peak amplitude (p.t.p.a.) of the light curve of 0.7 ± 0.1 mag, though it may be larger since we could not sample the entire rotational phase. With a model that assumes the nucleus is a triaxial ellipsoid with an angular momentum vector (a) initially pointing in the direction found by Sekanina (1988a) and (b) "precessing" in a circle due to a torque from the outgassing vents on the surface, we combined our dataset and the p.t.p.a. reported by JM87 and LJ90 to

find that the precession period is less than 81 years, one axial ratio a/c is at least 2.6, and the other one b/c satisfies $1.0 \leq b/c \leq 0.5 \times a/c - 0.3$. The precession circle's axis must be at least 14° from the angular momentum vector. We surmise that a significant mass ejection event could have occurred in the mid-1980s to start the angular momentum vector moving again, since, according to Sekanina (1988a), on average it was in the same place for much of the 20th century.

• 5. The nucleus' radius is toward the low end of known radii of nuclei, while the axial ratio is toward the high end (Meech 1999). The albedo is comparable to Halley's and not unlike the other few comets for which it has been measured (Chapter 9). Among known near-Earth asteroid properties, the radius is in the middle, and the albedo is on the low end. However the samples of comets and NEAs both suffer from incompleteness and observational bias.

• 6. Under the STM formalism, we can constrain neither the beaming parameter η nor the infrared phase coefficient β_i other than to say Encke's thermal behavior is consistent with the values found for these parameters from asteroids and icy satellites. Future studies of comet Encke's nucleus should try to employ a wide range of phase angles and a wider range of wavelengths to better understand its thermal phase behavior and improve the interpretation of radiometry.